Rousseau, D. L. (1981) *J. Raman Spectrosc. 10*, 94.
Rousseau, D. L., & Ondrias, M. R. (1985) *Biophys. J. 47*, 726.
Rousseau, D. L., Tan, S. L., Ondrias, M. R., Ogawa, S., & Noble, R. W. (1984) *Biochemistry 23*, 2857.
Scheidt, W. R., & Frisse, M. E. (1975) *J. Am. Chem. Soc. 97*, 17.
Scheidt, W. R., & Piciulo, P. L. (1976) *J. Am. Chem. Soc. 98*, 1913.
Schomaker, K. T., & Champion, P. M. (1986) *J. Chem. Phys. 84*, 5314.
Schomaker, K. T., Bangcharoenpaurpong, O., & Champion, P. M. (1984) *J. Chem. Phys. 80*, 4701.
Seilmeier, A., Scherer, P. O. J., & Kaiser, W. (1984) *Chem. Phys. Lett. 105*, 140.
Shaanan, B. (1983) *J. Mol. Biol. 171*, 31.
Shelby, R. M., Harris, C. B., & Cornelius, P. A. (1979) *J. Chem. Phys. 70*, 34.
Spiro, T. G., & Burke, J. M. (1976) *J. Am. Chem. Soc. 98*, 5482.
Terner, J., Stong, J. D., Spiro, T. G., Nagumo, M., Nicol, M. F., & El-Sayed, M. A. (1981) *Proc. Natl. Acad. Sci. U.S.A. 78*, 1313.
Tsubaki, M., & Yu, N.-T. (1982) *Biochemistry 21*, 1140.
Tsubaki, M., Nagai, K., & Kitagawa, T. (1980) *Biochemistry 19*, 379.
Tsubaki, M., Srivastava, R. B., & Yu, N.-T. (1982) *Biochemistry 21*, 1132.
Yamamoto, T., Palmer, G., Gill, D., Salmeen, I. T., & Rimai, L. (1973) *J. Biol. Chem. 248*, 5211.

Electron–Nuclear Coupling in Nitrosyl Heme Proteins and in Nitrosyl Ferrous and Oxy Cobaltous Tetraphenylporphyrin Complexes†

Richard S. Magliozzo,* John McCracken, and Jack Peisach
Department of Molecular Pharmacology, Albert Einstein College of Medicine, Bronx, New York 10461
Received April 29, 1987; Revised Manuscript Received July 2, 1987

ABSTRACT: Electron spin echo envelope modulation (ESEEM) spectroscopy has been used to study electron–nuclear interactions in the following isoelectronic $S = {}^1/_2$ complexes: NO–Fe^{II}(TPP) (TPP = tetraphenylporphyrin) with and without axial nitrogenous base, nitrosylhemoglobin in R and T states, and O_2–Co^{II}(TPP) with and without axial base. Only the porphyrin pyrrole nitrogens contribute to the ESEEM of the 6-coordinate nitrosyl Fe^{II}(TPP) complexes, nitrosylhemoglobin (R-state), and the nitrosyl complexes of α and β chains. Pyrrole nitrogens in the 5-coordinate complex NO–Fe^{II}(TPP) are coupled too weakly to unpaired spin and therefore do not contribute to the ESEEM. A partially saturated T-state nitrosylhemoglobin does not exhibit echo envelope modulations characteristic of 6-coordinate nitrosyl species, which confirms that the proximal imidazole bond to heme iron is disrupted. Study of 6-coordinate O_2–Co^{II}(TPP)(L) complexes (L = nitrogenous base) using ^{14}N- and ^{15}N-labeled ligands and porphyrins enabled a detailed analysis of coupling parameters for both pyrrole and axial nitrogens. The pyrrole ^{14}N coupling frequencies are similar to those in NO–Fe^{II}(TPP)(L). The Fermi contact couplings for axially bound nitrogen, calculated from simulation of ESEEM spectra for a series of O_2–Co^{II}(TPP)(L) complexes (L = pyridine, 4-picoline, 4-cyanopyridine, 4-carboxypyridine, and 1-, 2-, and 4-methylimidazole) illustrate a trend toward stronger hyperfine interactions with weaker bases.

The magnetic resonance properties of metalloporphyrin complexes can often provide insight into the biochemistry of heme proteins. An understanding of the interactions between unpaired electron spin and nearby nuclei in metalloporphyrins enables the spectroscopist to address the effects on these interactions imposed by the protein in which the metalloporphyrin resides and to relate the prosthetic group properties to the tertiary and quaternary structure of that protein.

Electron paramagnetic resonance spectroscopy has been extensively used in studies of high- and low-spin ferric heme proteins (Blumberg et al., 1968; Peisach et al., 1971; Chevion et al., 1977; Hollenberg et al., 1980; Palmer, 1985) and ferrous nitrosyl heme proteins (Kon, 1968; Yonetani et al., 1972; Chevion et al., 1977; Hille et al., 1979; Morse & Chan, 1980; Hori et al., 1981; LoBrutto et al., 1983). These studies, in general, have addressed the identity of axial ligands to heme iron. An application of EPR[1] and ENDOR techniques to the chemistry of allosterism in hemoglobin has provided evidence for the disruption of the proximal imidazole Fe–N bond in the α subunits of nitrosylhemoglobin A in the low-affinity form, or T state (Höhn et al., 1983). The lability of this bond is suggested by a body of evidence for nitrosylhemoglobins (Szabo & Perutz, 1976; Nagai et al., 1980; Ascenzi et al., 1981).

Pulsed EPR techniques and the observation of electron spin echo modulations can also be used to study the biochemistry of hemoglobin. Electron spin echo envelope modulation spectroscopy, in its application to high- and low-spin d^5 heme proteins and iron metalloporphyrins, allows assignment of

† This work was supported by Grants HL-13399 and RR-02583 from the National Institutes of Health.

[1] Abbreviations: EPR, electron paramagnetic resonance; ENDOR, electron nuclear double resonance; ESEEM, electron spin echo envelope modulation; TPP, tetraphenylporphyrin; PPIX, protoporphyrin IX; imid, imidazole; pyr, pyridine; IHP, inositol hexaphosphate; Hb, hemoglobin; NQR, nuclear quadrupole resonance; nqi, nuclear quadrupole interaction; PAS, principal axis system; DEAE, dimethylaminoethyl; Tris, tris(hydroxymethyl)aminomethane.

0006-2960/87/0426-7923$01.50/0

frequencies arising from electron–nuclear interactions with axial and equatorial ligands to iron (Peisach et al., 1979). These hyperfine effects can be investigated by ESEEM when the weak interactions are not resolved by conventional continuous wave EPR techniques. ESEEM spectroscopy can also be applied in the study of electron–nuclear interactions in $S = {}^1/_2$ complexes containing low-spin d^6 or d^7 metal ions. Examples of these are nitrosyl ferrous heme proteins and NO–heme–(L) complexes (Peisach et al., 1979; Peisach, 1982) and the isoelectronic oxygenated cobaltous porphyrin complexes. In these cases, ESEEM spectroscopy is especially well suited to the investigation of weak couplings between the unpaired spin delocalized from the NO and O_2 ligands and the metal-coordinated nitrogen atoms.

In this paper, ESEEM spectroscopy was used to study 5- and 6-coordinate nitrosyl–iron–TPP complexes, nitrosyl α and β chains of hemoglobin A, and fully and partially ligated nitrosylhemoglobin. One aim of this study was a search for proximal imidazole nitrogen coupling in low-affinity nitrosylhemoglobin that differed from the couplings in the high-affinity form (R state) and in iron nitrosyl model compounds. The present investigation readdresses the assignment of frequencies reported earlier for nitrosyl heme complexes (Peisach, et al., 1979; Peisach, 1982) and provides further evidence for the dissociation of the proximal imidazole in α subunits of T-state nitrosylhemoglobin.

The substitution of Co(II) for iron in heme proteins provides a paramagnetic probe useful for the elucidation of protein structure. As a background for future study of electron–nuclear coupling in CoPPIX-substituted heme proteins, we report an ESEEM study of O_2–Co^{II}(TPP)(L) complexes. The results revealed axial base effects that were not amenable to study in the nitrosyl complexes. Contact couplings calculated from frequency data for a series of O_2–Co^{II}(TPP)(L) complexes are presented and show a trend toward stronger coupling for weaker base donors. The quadrupolar parameters for axial nitrogens, calculated from simulation of ESEEM data, compared well to those reported in NQR studies of crystalline complexes of Zn(II) with pyridine and imidazole (Ashby et al., 1978; Hsieh et al., 1977).

Materials and Methods

Sample Preparation. NO–Fe^{II}(TPP) was synthesized from commercial Fe(TPP)Cl (Porphyrin Products) according to a published method (Scheidt & Frisse, 1975) using glassware sealed with serum caps and fitted with hypodermic needles for gas exchange. The purple crystals of NO–Fe^{II}(TPP) were collected from the reaction mixture and were used without recrystallization. The EPR spectrum (77 K) of the product dissolved anaerobically in toluene did not show any high-spin iron signal, which indicates a quantitative reduction of ferric iron and conversion to NO–Fe^{II}(TPP).

Methanol was distilled over Mg. Nitric oxide was passed through NaOH pellets before use. Toluene was dried with $CaCl_2$ and was distilled from sodium. 4-Cyanopyridine was recrystallized twice from toluene (mp 80 °C). [^{15}N]Pyridine was purchased from Prochem and was used without purification. [^{14}N]Imidazole was recrystallized from benzene, and 2-methylimidazole was recrystallized from chloroform. 4-Picoline was dried over $CaCl_2$ and was purified by distillation under N_2 (bp 143 °C).

Samples of the 6-coordinate NO–Fe^{II}(TPP)(L) complexes (final concentration 1–2 mM) were prepared anaerobically in sidearm test tubes. After thorough degassing with N_2, toluene or toluene with added ligands (L = [^{14}N]- and [^{15}N]pyridine, imidazole, 2-methylimidazole) was tipped from the central compartment of the tube into the sidearm to dissolve the NO–Fe^{II}(TPP). [The solvent for the imidazole complexes was 10% methanol in toluene (v/v).] Samples were loaded into N_2-purged EPR tubes sealed with serum stoppers by using a gastight syringe. The solutions were immediately frozen by immersion in liquid N_2. All samples were prepared with a large excess of ligand.

Hemoglobin A, isolated from blood freshly drawn from laboratory personnel, was prepared according to a modification of a published procedure (Carrico et al., 1978). Hemolysate, prepared from washed red cells by osmotic shock, was freed of cell debris by centrifugation. The centrifugate was chromatographed on DEAE-cellulose (Whatman DE-53) at pH 8.1, and after concentration by ultrafiltration, the oxyhemoglobin was rechromatographed on Sephadex G-100 and was subsequently stripped of organic phosphates (Bonaventura & Bonaventura, 1981) by chromatography on Sephadex G-25 equilibrated with 0.05 M Tris-HCl, pH 8.1, containing 0.1 M KCl. The purified protein was subsequently chromatographed through Chelex 100 equilibrated with the same buffer to remove adventitious metal ions.

Hemoglobin α and β chains were prepared according to a published procedure (Bucci, 1981) and were reduced to their free sulfhydryl forms by treatment with either dithiothreitol (Ikeda-Saito et al., 1981) (α chains) or 2-mercaptoethanol (Geraci et al., 1969) (β chains). The sulfhydryl content was checked by optical titration with *p*-mercuribenzoate (Boyer, 1954) and was found to be stoichiometrically correct for both chains (1 sulfhydryl/α chain, 2 sulfhydryl/β chain). All purified proteins were concentrated by ultrafiltration and were stored under liquid N_2.

Nitrosyl derivatives of heme proteins were prepared in 0.2 M Tris-HCl, pH 8.1, from carboxy chains or from oxyhemoglobin A by equilibration of anaerobic solutions with NO at 1 atm. A T-state nitrosyl derivative (Hille et al., 1979) was prepared by diluting 4 mM oxyhemoglobin (in 0.05 M Tris buffer, 0.1 M KCl, pH 8.1) with an equal volume of 15 mM IHP (in 0.2 M Tris buffer titrated to pH 6.2 with HCl). The final pH of a sample diluted in this way was near 6.5. After thorough deaeration, the deoxygenated sample (300 μL) was transferred to a nitrogen-purged, 500-μL centrifuge tube sealed with a serum cap. A 30-μL portion of NO-saturated buffer (0.2 M Tris-HCl, pH 6.2, containing 15 mM IHP) was then added to the hemoglobin, leaving little dead space above the solution. This mixture, which contained enough NO to saturate approximately 10% of the total heme, was incubated for 30 min at room temperature. The solution was then transferred to a deaired EPR tube and was immediately frozen in liquid nitrogen.

Co^{II}[[^{15}N](TPP)] was a gift from Dr. A. Adler. Solutions of oxygenated Co^{II}(TPP) complexes were prepared by dissolving Co^{II}[[^{14}N]- or [^{15}N](TPP)] in toluene (final concentration approximately 1 mM) in air. Oxygenated complexes with nitrogenous axial bases were prepared by dissolving Co^{II}(TPP) in toluene containing 30% pyridine, 30% 4-picoline, or 10% 1-methylimidazole (v/v). The 2-methylimidazole, 4-methylimidazole, 4-carboxypyridine, and 4-cyanopyridine complexes were prepared by adding methanol saturated with ligand to Co^{II}(TPP) in toluene to give a final solvent mixture containing 1:10 methanol–toluene. These solutions were transferred to EPR tubes and were frozen by immersion in liquid nitrogen for examination by both continuous wave and pulsed EPR techniques. Continuous wave EPR spectra recorded at 77 K did not contain signals other than those characteristic of the 6-coordinate oxy complexes, which in-

dicates that the 2:1 axial base adducts were not present in the samples (Walker, 1970).

Spectroscopy. Continuous wave EPR spectra were recorded with a Varian E-112 spectrometer equipped with a Polytechnic Research and Development Co. wavemeter and a Varian NMR gaussmeter. A liquid nitrogen cold finger was used to hold samples for continuous wave EPR spectra recorded at 77 K, and a Heli-Tran liquid helium transfer apparatus (Air Products) was used in recording spectra at 6 K. The pulsed EPR spectrometer used to obtain electron spin echo envelope data at 4 K has been described elsewhere (McCracken et al., 1987a). Two microwave cavity systems were used for the measurements reported here. A stripline transmission cavity (Mims, 1974) was used in some experiments at 9 GHz and for all the investigations at 11 GHz. For model compound studies at 9 GHz, a reflection cavity system was also used. This cavity employs a folded stripline as the resonant element (Lin et al., 1985) and a coupling scheme suited for use in a cryogenic immersion Dewar (Britt & Klein, 1987). When necessary, an anaerobic chamber was used to hold the stripline transmission cavity during sample loading and freezing.

As in previous pulsed EPR studies, electron spin echo envelopes were obtained by using the two-pulse and three-pulse or "stimulated echo" methods (Mims & Peisach, 1979; Peisach et al., 1979). Echo envelopes were extrapolated to "zero time" and Fourier transformed in order to obtain the frequency spectra presented throughout this work (Mims, 1984). Three-pulse echo envelopes were generally recorded with the time interval between the first two pulses (τ) chosen to suppress the proton frequency (Peisach et al., 1979). Interpretation of frequency data was often facilitated by examining Fourier transforms of data recorded at both 9 and 11 GHz at the same experimental g value.

Calculations. Magnetic coupling parameters for O_2–Co^{II}(TPP)(L) were compared to modulation functions obtained from computer simulations using the density matrix formalism developed by Mims (Mims, 1972) and applied by Reijerse and Keijzers (1987). The general expression for a stimulated echo envelope modulation function is given by

$$E_{mod}(\tau,T) = [2(2I + 1)]^{-1} \text{ Tr } \{G_\alpha + G_\beta\}$$

where

$$G_\alpha = Q_\tau^\dagger M^\dagger P_T^\dagger P_\tau^\dagger M Q_\tau M^\dagger P_T P_\tau M$$

$$G_\beta = Q_\tau^\dagger Q_T^\dagger M^\dagger P_\tau^\dagger M Q_\tau Q_T M^\dagger P_\tau M \quad (1)$$

Q, P, and M in eq 1 are matrices of dimension $2I + 1$, with P and Q being submatrices of the rotation operators that describe the time evolution of the density matrix during the free-precession periods for the two electron spin manifolds. The modulation depths of the superhyperfine frequencies contained in P and Q are given by the elements of M, where

$$M = M_\alpha^\dagger M_\beta \quad (2)$$

M_α and M_β are matrices that diagonalize the spin Hamiltonian that describes the superhyperfine splittings in the $+^1/_2$ and $-^1/_2$ electron spin manifolds, respectively.

The Hamiltonian used to model the superhyperfine splittings for the ^{15}N data presented below consists of terms describing the nuclear Zeeman and electron–nuclear hyperfine interactions and is given by

$$H_N = \sum_{i=x,y,z} (m_s A_{ii} - \nu_n) l_i \hat{I}_i \quad (3)$$

where the terms A_{ii} are the elements of the hyperfine tensor, ν_n is the nuclear Zeeman frequency at the magnetic field strength of the experiment, the l_i are the direction cosines relating the direction of the applied static magnetic field to the principal axis system of the hyperfine tensor, and the $\hat{I}_i$ are the nuclear spin operators. Implicit in eq 3 is an isotropic g tensor and the assumption that the Hamiltonian is evaluated in the PAS of the hyperfine coupling tensor. The Hamiltonian matrix for an $I = {}^1/_2$ nucleus is easily diagonalized, and analytical solutions for eq 1 have been developed (Mims, 1972; Kevan, 1975). For all simulations, an average over all possible orientations of the magnetic field direction with respect to the hyperfine PAS was performed. This spherical averaging is valid for the simulation of ESEEM for O_2–Co^{II}(TPP)(L) complexes because of the small g-tensor anisotropy and the large hypefine coupling for the $I = {}^7/_2$ Co nucleus (approximately 18 G) (Hoffman et al., 1970).

Simulation of ESEEM due to ^{14}N nuclei requires that the nuclear quadrupole interaction also be considered in the spin Hamiltonian. The additional term is given by

$$H_Q = (e^2qQ/4)[(3\hat{I}_z'^2 - 2) + \eta(\hat{I}_x'^2 - \hat{I}_y'^2)] \quad (4)$$

Five parameters are needed to model the nqi: e^2qQ, the quadrupole coupling constant; η, the asymmetry parameter; and the three Euler angles α, β, and γ, which describe the relationship between the principle axes of the hyperfine and nqi tensors. The nuclear spin operators in eq 4 are primed because they refer to the nqi PAS, while those of eq 3 refer to the hyperfine PAS.

The addition of eq 4 to the spin Hamiltonian precludes the development of exact analytical solutions for the modulation function (eq 1) and requires that the simulations be performed numerically. In an ESEEM calculation, the Euler angle rotation of the nqi spin operator is carried out first, and then this "effective" set of nqi parameters is used along with the remainder of H_N to calculate the Hamiltonian matrix for both electron spin sublevels. The two matrices are then diagonalized, and the eigenvalues are used to compute the elements of P and Q, while the eigenvectors are used to set the elements of M. The results are then used in eq 1, and the modulation function for a given set of direction cosines, l_i, is computed. This procedure, except for the Euler angle rotation, is then repeated for all possible orientations of the static magnetic field direction with respect to the PAS of the hyperfine coupling tensor in order to obtain a powder average modulation function. The input parameters for a calculation are the following: g_n, the nuclear g value; A_{xx}, A_{yy}, and A_{zz}, the elements of the hyperfine tensor; H_0, the magnetic field strength used in the measurement; the timing parameters used in the measurement; and the parameters describing the nqi.

Results and Discussion

Nitrosyl Fe^{II}(TPP) and Heme Complexes. The Fourier transform of the three-pulse spin echo envelope for the pentacoordinate complex NO–Fe^{II}(TPP) and the continuous wave EPR spectrum for the same complex are shown in Figure 1A. The unpaired spin of the axial NO ligand is strongly coupled to its ^{14}N nucleus as evidenced by the 17-G splitting at g_z (g = 2.01). Nitrogen nuclei having hyperfine interactions of this magnitude do not contribute to ESEEM (Mims & Peisach, 1978).

The featureless ESEEM spectrum suggests that the pyrrole nitrogen atoms of the porphyrin are too weakly coupled to the unpaired spin in the complex to contribute to the spin echo envelope. Calculations (Mun et al., 1979) predict that pyrrole nitrogen couplings should be less than 3 G (9 MHz) and could therefore be in a range expected to give rise to ESEEM. The data in Figure 1A suggest that the Fermi contact coupling to the pyrrole nitrogens is considerably smaller and, on the basis

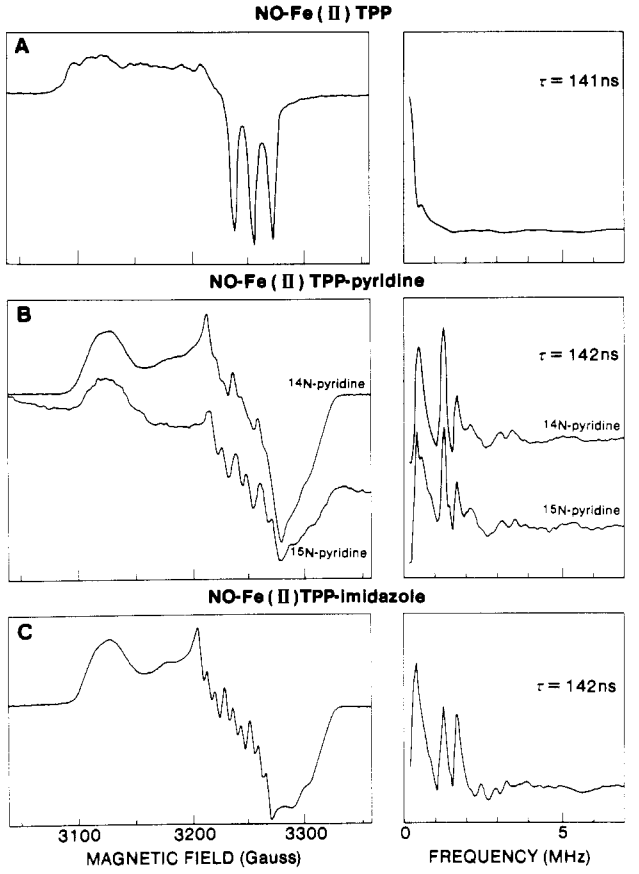

FIGURE 1: Continuous wave EPR spectra (left) and ESEEM spectra (Fourier transforms) (right) for 5- and 6-coordinate NO–Fe^{II}(TPP) complexes: (A) NO–Fe^{II}(TPP); (B) NO–Fe^{II}(TPP)[[^{14}N]pyridine or [^{15}N]pyridine]; (C) NO–Fe^{II}(TPP)(imidazole). Sample preparation is described under Materials and Methods. Experimental conditions for EPR spectra were as follows: frequency, 9.1 GHz, microwave power, 5 mW; modulation amplitude, 1.0 G; temperature, 77 K. Experimental conditions for ESEEM spectroscopy were as follows: frequency, 9.6 GHz; magnetic field, 3330 G; τ, 141 ns; temperature, 4.2 K. The choice of other parameters is described under Materials and Methods. The spectra, obtained by cosine Fourier transform, are plotted with approximately equal amplitude scales in all cases.

of a spectral simulation (not shown), is probably less than 0.5 MHz.

NO–Fe^{II}(TPP) dissolved in toluene containing pyridine forms a hexacoordinate species with pyridine nitrogen as an axial ligand. The continuous wave EPR spectrum of this complex (Figure 1B, left) is characterized by a nine-line superhyperfine pattern at g_z (Kon, 1975) arising from the coupling of unpaired spin to two axial ^{14}N (I = 1) nuclei. A similar sample prepared with [^{15}N]pyridine ($I = {}^1/_2$) exhibits a six-line superhyperfine pattern (Figure 1B, left). The splitting of approximately 22 G in both spectra is due to the hyperfine interaction attributable to the ^{14}N of the NO ligand. The multiplicity of the additional splittings indicates coupling to the I = 1 or $I = {}^1/_2$ nitrogen atoms of the pyridine ligands.

The Fourier transforms of spin echo envelopes for the [^{14}N]- and [^{15}N]pyridine complexes are nearly identical and contain frequency components equal to 0.4, 1.3, and 1.7 MHz (Figure 1B, right). These components must arise from couplings to the pyrrole nitrogens of the porphyrin since isotopic substitution of axial ligand does not change the ESEEM spectrum.

The NO–Fe^{II}(TPP)(L) complex prepared with imidazole as the sixth ligand exhibits a continuous wave EPR spectrum similar to that found for the pyridine complex but with better resolution of the nine-line superhyperfine pattern (Figure 1C, left). This complex exhibits the same ESEEM frequencies as the pyridine complexes (Figure 1C, right). A hexacoordinate NO complex prepared with 2-methylimidazole also shows the same frequencies (data not shown).

ESEEM investigations of $S = {}^1/_2$ complexes with weak coupling of electron spin to nitrogen nuclei of ligands often reveal three low-frequency components with two frequency values that add up to the third. The frequencies depend on the ^{14}N Zeeman energy (0.3 MHz/kG), the nuclear quadrupole interaction, and the hyperfine field arising both from the transfer of unpaired spin (contact) and from anisotropic dipolar interactions (Mims & Peisach, 1978). In certain cases, the Zeeman interaction is nearly canceled in one of the EPR spin states by the hyperfine interactions at the nitrogen nucleus of interest. The zero-field condition is then approximated for this nitrogen, and the resulting energy level splittings for the electron spin manifold are mostly determined by the nqi. The similarity of frequency components observed for the three hexacoordinated complexes where L = pyridine, imidazole, or 2-methylimidazole indicates that the coupling of the electron spin to pyrrole nitrogens is nearly the same, though the axial hyperfine interaction may be slightly altered. The zero-field nuclear quadrupole transition energies have been reported for pyrrole ^{14}N of crystalline CuTPP (0.313, 1.233, 1.545 MHz) and AgTPP (0.470, 1.137, 1.607 MHz) (Brown & Hoffman, 1980). These values are close to the frequencies observed in Fourier transforms of the ESEEM of NO–Fe^{II}(TPP)(L) complexes presented here and corroborate their assignment to the pyrrole nitrogens of the porphyrin.

Two higher frequency components are observed in Fourier transforms of most ESEEM data for NO–Fe^{II}(TPP)(L) complexes, including those prepared with ^{15}N-labeled pyridine. These frequencies, at 3 and 5.5 MHz, are also assigned to the pyrrole nitrogens and may arise from couplings to nuclear transitions for which the hyperfine field adds to the Zeeman field at the nitrogen nucleus.[2] The frequency data obtained for NO–Fe^{II}(TPP)(L) complexes are quite similar to the ESEEM data for O_2–Co^{II}(TPP)(L) complexes discussed below, and the simulation of modulation components and complete assignments are reserved for the latter complexes.

Coupling to the directly coordinated and remote nitrogen atoms of bound imidazoles is not detected by ESEEM spectroscopy since no new components were observed upon substitution of imidazole for pyridine. ENDOR spectroscopy indicates a 16-MHz coupling for the directly coordinated, or imino, nitrogen of imidazole in nitrosyl heme proteins and NO heme model complexes (LoBrutto et al., 1983). Couplings of this magnitude do not give rise to envelope modulations in our spin-echo experiments (Mims & Peisach, 1978). The ESEEM results are also consistent with a very small hyperfine interaction at the remote or amino nitrogen nucleus, predicted theoretically to be less than 1 G (3 MHz) in hexacoordinate NO–iron porphyrin complexes (Mun et al., 1979). Hyperfine interaction at the amino ^{14}N is observed for Cu^{II}(imid) complexes, however, when the directly coordinated ^{14}N coupling is approximately twice as large as in the porphyrin complexes examined here (Mims & Peisach, 1978; Van Camp et al., 1981).

Failure to observe ESEEM from the remote nitrogen of imidazole in NO–Fe^{II}(TPP)(imid) allows a refinement of the theoretical predictions by Mun et al. (1979). Computer simulations of ESEEM patterns for a weakly coupled nitrogen were performed with the protocol given above and the nqi

[2] It is also possible that the 3-MHz component contains a sum frequency line arising from the interaction of multiple ^{14}N nuclei having similar couplings (Kosman et al., 1980; McCracken et al., 1987b).

parameters for the amino nitrogen of imidazole reported by Ashby et al. (1978). It was found that the predicted modulation depths were too shallow to be resolved (less than 3% of the echo amplitude) for the case where a long-range dipolar interaction was used to formulate the hyperfine tensor anisotropy when the Fermi contact term was less than 0.6 MHz. Considering the signal to noise ratio for our measurements and the fact that no background decay functions were included in the above simulations, the failure to observe ESEEM from the remote nitrogen indicates that the contact coupling for this nucleus must be less than 0.6 MHz. ESEEM theory predicts that the limitation in spectral resolution could be extended if the experiments were performed at a lower microwave frequency and field strength. For example, when the above simulations are done assuming a magnetic field strength of 2100 G (g = 2 at approximately 6 GHz), the predicted modulations depths for a = 0.6 MHz would be about 10%.

In an earlier ESEEM study of NO–heme–imidazole, frequency components of 0.7, 1.4, and 4.0 MHz were assigned to imidazole amino nitrogen couplings (Peisach et al., 1979). These frequencies were significantly different from those reported for nitrosylmyoglobin (Peisach et al., 1979) but are similar to those observed for Cu^{II}(imid) complexes (Mims & Peisach, 1978). The earlier results for the NO–heme–(imid) complex are not consistent with current data for samples that have the continuous wave EPR spectrum of a single species, the hexacoordinate NO–Fe^{II}(TPP)(imid) complex. The early study did not report continuous wave EPR spectra for the NO–heme–(imid) sample since the microwave cavity used for the measurements did not permit study of a given sample by both continuous wave and pulsed EPR methods. The frequencies reported earlier are observed in ESEEM of samples containing methemoglobin (data not shown). It is likely that the frequencies originally reported for NO–heme–(imid) actually arose from the imidazole ligand bound in a high-spin Fe(III)–heme–(imid) complex. The differences between current ESEEM data and the early report cannot be ascribed to the differences between heme and TPP nor to the different solvents used since in the present study the data for the model complexes dissolved in toluene match the data for nitrosyl heme proteins.

Nitrosylhemoglobin. Nitrosyl derivatives of isolated subunits of hemoglobin A (NO–α chains, NO–β chains) and stripped nitrosylhemoglobin, $Hb(NO)_4$, in phosphate-free buffer have also been examined. The continuous wave EPR spectrum as well as the ESEEM spectrum for fully ligated $Hb(NO)_4$ are shown in Figure 2A. The frequency components in the Fourier transform are comparable to those for 6-coordinate NO–Fe^{II}(TPP)(L) complexes prepared with pyridine or imidazole and are also similar to those for nitrosyl α and β chains (data not shown). The results indicate similar magnetic coupling to pyrrole nitrogens in the hexacoordinate NO–heme prosthetic groups of these proteins and in the NO–Fe^{II}(TPP)(L) models.

The structural differences between the model complexes and the prosthetic groups in the proteins are expected to involve restraints on the Fe–NO bond angle and the orientation of the axial imidazole plane. Structural changes imposed by the proteins could alter the distribution of unpaired spin through changes in axial bonds, but only small changes in the already weak interaction with pyrrole nitrogens would be expected. ENDOR spectroscopy of fully ligated $Hb(NO)_4$ (Höhn et al., 1983) indicates some small differences in the hyperfine interaction with the directly coordinated nitrogen of the proximal imidazole in α compared to β NO chains in the fully ligated

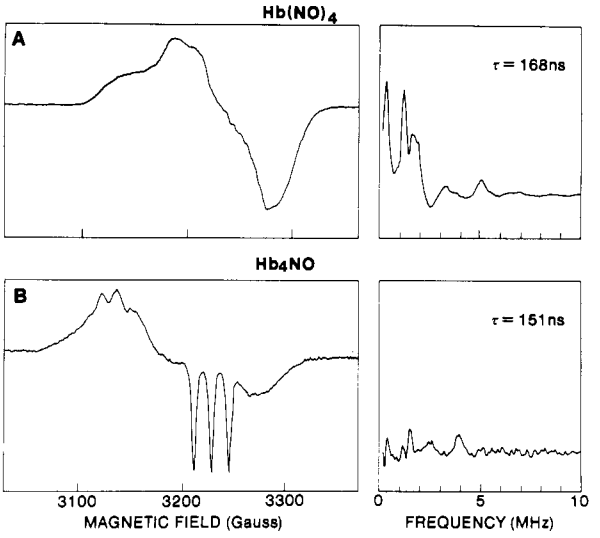

FIGURE 2: Continuous wave EPR spectra (left) and ESEEM spectra (right) for fully ligated nitrosylhemoglobin [$Hb(NO)_4$] and partially saturated nitrosylhemoglobin with IHP (Hb_4NO): (A) stripped nitrosylhemoglobin in Tris-HCl buffer, pH 8; (B) partially saturated nitrosyl hemoglobin in Tris-HCl buffer, pH 7, containing 15 mM IHP. Sample preparation is described under Materials and Methods. Experimental conditions for EPR spectra were as follows: (A) frequency, 9.1 GHz; modulation amplitude, 2.5 G; microwave power, 1.0 mW; temperature, 77 K; (B) frequency, 9.1 GHz; modulation amplitude, 2 G; microwave power, 4.0 mW; temperature, 77 K. Experimental conditions for ESEEM spectroscopy were as follows: (A) frequency, 8.9 GHz; magnetic field, 3175 G; (B) frequency, 8.9 GHz; magnetic field, 3120 G. ESEEM data were normalized prior to Fourier transformation and are plotted with equivalent amplitude scales. The set of frequencies found in the data shown in (B) corresponds to the nitrogen couplings found for high-spin aquo ferric heme, as in metmyoglobin (Peisach et al., 1984).

nitrosyl tetramer, but no such effects for the pyrrole nitrogens are seen in ESEEM spectra.

ESEEM studies of models, isolated nitrosylhemoglobin chains, and fully ligated nitrosylhemoglobin in the high-affinity form (R state) provide frequency markers for 6-coordinate nitrosyl complexes and therefore provide a background for investigating the effects of quaternary structural changes in nitrosylhemoglobin. Figure 2B (right) shows an ESEEM Fourier transform for a partially saturated nitrosyl-Hb sample (Hb_4NO) in the presence of the allosteric modifier inositol hexaphosphate. The continuous wave EPR spectrum of this low-affinity Hb sample (Figure 2B, left) has a three-line superhyperfine pattern which indicates that the 5-coordinate complex, similar to NO–Fe^{II}(TPP), is the majority NO-ligated species (Hille et al., 1979; Szabo & Perutz, 1976), though some contamination by metHb was found in an EPR spectrum recorded at 6 K (data not shown). The method of preparation of this partially saturated hemoglobin sample allows the NO ligand to equilibrate on α chains only, where it induces a dissociation of the proximal imidazole from the iron in those subunits of the T-state tetramer (Hille et al., 1979). The ESEEM spectrum is *atypical* of 6-coordinate nitrosyl complexes. The absence of pyrrole nitrogen coupling frequencies indicates conversion of the nitrosyl hemes to a pentacoordinate structure. Dissociation of the proximal imidazole from heme iron is consistent with an ENDOR study (Höhn et al., 1983) in which the frequency components assigned to the nitrogen of proximal imidazole in α chains of $Hb(NO)_4$ are absent when the protein is converted to the T state.

Oxygenated Co^{II}(TPP) Complexes. The couplings to pyrrole ^{14}N in NO–Fe^{II}(TPP)(L) complexes are in a frequency range amenable to study by ESEEM methods. The axial nitrogen couplings in these complexes are considerably larger

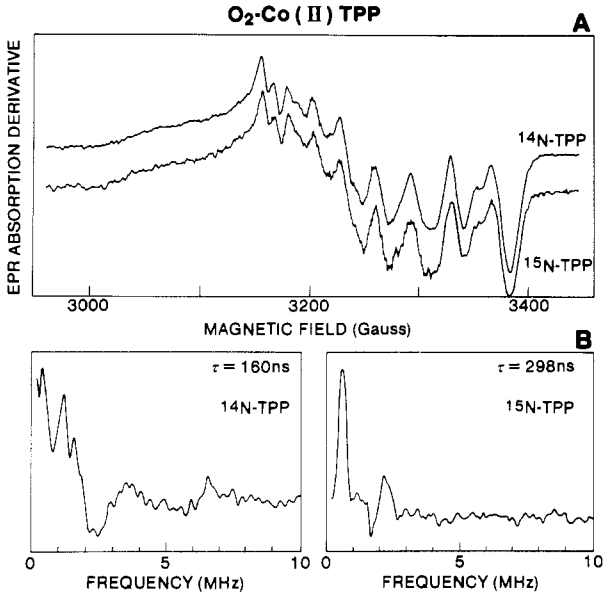

FIGURE 3: EPR spectra (A) and ESEEM spectra (B) for O_2–Co^{II}(TPP). Experimental conditions for EPR spectra were as follows: frequency, 9.1 GHz; modulation amplitude, 1.0 G; microwave power, 5.0 mW; temperature 77 K. Experimental conditions for ESEEM spectroscopy were as follows: frequency, 9.0 GHz; magnetic field, 3150 G.

and can be investigated by continuous wave EPR methods. The 6-coordinate oxygenated Co(II) porphyrin complexes, which are isoelectronic with the NO–Fe(II) complexes, exhibit weak axial nitrogen couplings, and ESEEM spectroscopy provides an excellent method for examination of both pyrrole and axial nitrogen interactions.

The continuous wave EPR spectrum of O_2–Co^{II}(TPP) in toluene, in the absence of added exogenous nitrogen ligands, exhibits hyperfine lines arising from ^{59}Co ($I = {}^7/_2$). Nitrogen hyperfine features arising from pyrrole nitrogens are not resolved. Figure 3A illustrates that the continuous wave EPR spectra of O_2–Co^{II}[[^{14}N](TPP)] and O_2–Co^{II}[[^{15}N](TPP)] in toluene are identical. The ESEEM spectra (Figure 3B) show components at 0.3, 1.2, 1.6, 3.4, and 6.4 MHz that are assigned to pyrrole ^{14}N couplings. [For the O_2–Co^{II}[[^{15}N](TPP)] case, only two components are seen (0.6 and 2.2 MHz at 3150 G).] The ^{14}N frequencies are similar to those assigned to pyrrole nitrogen in the NO–Fe^{II}(TPP)(L) complexes discussed above, suggesting that the structure of the Co^{II}(TPP) complexes in toluene are 6-coordinate, possibly because of axial ligation by trace H_2O (Hoffman et al., 1970).[3] The component that appears at 6.4 MHz in data recorded at a magnetic field of 3000 G ($g = 2.0$) appears at 6.8 MHz at a magnetic field of 3800 G (at the same g value). The shift in frequency of this component is twice the increase in Zeeman energy and indicates that the transition arises from the ^{14}N hyperfine manifold in which the nuclear hyperfine and Zeeman effects are additive (McCracken et al., 1987a,b). The other frequency components in the ESEEM spectrum shift only slightly (approximately 0.1–0.2 MHz) upon an increase in H_0 from 3000 to 3800 G.

The addition of nitrogenous bases to O_2–Co^{II}(TPP) in toluene yields 6-coordinate O_2–Co^{II}(TPP)(L) complexes (Walker, 1970; Stynes et al., 1973; Wayland et al., 1974; Drago et al., 1978; Rillema et al., 1982) whose EPR spectra exhibit ^{59}Co nuclear hyperfine couplings smaller than those in complexes where the sixth ligand is hydroxyl oxygen as found in a methanol complex (data not shown). Hyperfine interactions at the axial nitrogen are weak because unpaired spin density is associated mainly with the O_2 ligand in these complexes (see below).

Continuous wave EPR spectra of O_2–Co^{II}(TPP)(L) prepared with [^{14}N]- or [^{15}N]pyridine (Figure 4E) are indistinguishable, as are the corresponding spectra of complexes prepared with ^{15}N-labeled Co^{II}(TPP) (data not shown), because the only hyperfine interaction resolved in the spectra arises from ^{59}Co coupling. Since no measurement had ever been made of the nitrogen hyperfine interactions in these Co(II) complexes, it was of considerable interest to compare the pyrrole nitrogen couplings here to those in NO–Fe^{II}(TPP)(L) complexes and to follow trends in nitrogen couplings as a function of the axial base ligand.

Figure 4 shows ESEEM spectra for O_2–Co^{II}[[^{14}N]- and [^{15}N](TPP)](L) (L = [^{14}N]- or [^{15}N]pyridine). The frequencies that clearly arise from coupling to axial ^{14}N are those at 3.0 and 5.8 MHz since these are absent from spectra for the complex containing [^{15}N]pyridine (Figure 4A,B). When the ESEEM measurement for O_2–Co^{II}[[^{15}N](TPP)](pyr) is repeated at a higher microwave frequency (11 GHz) and magnetic field strength, keeping the effective g value constant, the pyridine ^{14}N components appear at 2.8 and 6.2 MHz. The magnetic field dependence indicates that these two frequency components arise from different electron spin manifolds and that the magnitude of the Fermi contact interaction for pyridine nitrogen is greater than twice the energy level splitting due to the nuclear Zeeman term (McCracken et al., 1987b). The frequency of these two components was also found to be sensitive to the nature of para substituents in the series of pyridine complexes described below.

Spectral Simulation. To provide a foundation for a more detailed comparison of magnetic coupling for pyridine complexes, the ESEEM spectra were simulated by using the formalism presented under Materials and Methods. The calculations focused primarily on predicting the frequencies, relative amplitudes, damping factors, and magnetic field dependence of the two higher frequency components and gave less consideration to the minor modulation components found at low frequency, where there is interference from the pyrrole nitrogen couplings. An NQR study of a variety of Zn(II)–pyridine complexes (Hsieh et al., 1977) revealed that both e^2qQ and η for pyridine ^{14}N decreases upon coordination to Zn(II). For free ligand, the e^2qQ and η values are 4.6 MHz and 0.4, respectively (Guibe, 1961), while for the Zn(II)-coordinated ligand these parameters were approximately 2.9 MHz and 0.2, respectively. Similar effects were found in an NQR study of metal-coordinated imidazoles (Ashby et al., 1978). These changes were analyzed within the framework of the Townes–Dailey model (Townes & Dailey, 1949) and correlated with the decreased orbital occupancy that occurs upon coordination to the metal: donation of the lone pair electrons leads to a reduction in the electric field gradient at the nitrogen nucleus, reducing e^2qQ. In addition, inductive effects cause the electron density for other orbitals of the pyridine nitrogen to increase, altering the asymmetry of the electric field gradient upon coordination to metal. A decrease in e^2qQ for the pyridine ^{14}N is also expected upon coordination in the O_2–Co^{II}(TPP)(pyr) complex, though changes in the asymmetry parameter are more difficult to predict due to the influence

[3] When toluene that had been saturated with H_2O or D_2O was used as solvent, the EPR and ESEEM spectra were the same as those recorded for samples in toluene distilled from Na. No change was observed in the EPR or ESEEM spectra when samples were dissolved in freshly distilled toluene under a stream of dry air. If these complexes are 6-coordinate, with an axial water ligand, the coupling to the axial hydrogens (deuterons) is too weak for observation of the deuterium modulation.

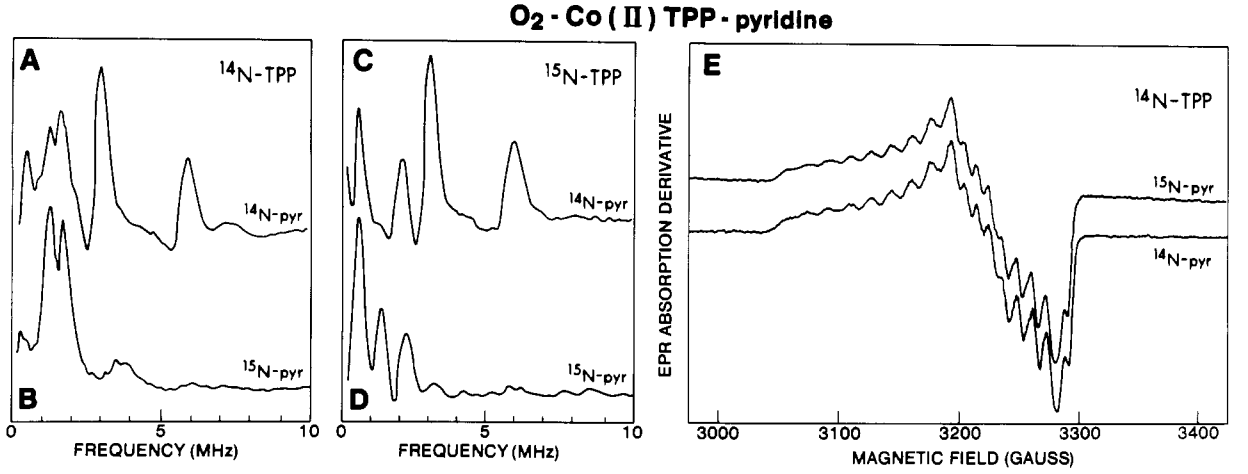

FIGURE 4: EPR spectra and ESEEM spectra for O_2–Co^{II}(TPP)(pyridine) complexes. Isotopic labeling is indicated in the figure. Experimental conditions for EPR spectra were as follows: frequency, 9.1 GHz; modulation amplitude, 1.0 G; microwave power, 5.0 mW; temperature, 77 K. Experimental conditions for ESEEM spectra were as follows: frequency, 9.0 GHz; magnetic field, 3060 G.

of π bonding expected for these compounds.

Two models were considered for the relationship between hyperfine and quadrupole tensors needed for the calculation of ESEEM parameters. The first model considered the principal axis of the two tensors to be aligned, the hyperfine principal axis being directed along the Co(II) d_{z^2} orbital and the principal axis of the nqi tensor being defined by the pyridine nitrogen hybrid orbital that contains the lone pair. In this model, electron donation from the axial base to Co(II) is assumed to be similar to that in the Zn(II)–pyridine complexes (Hsieh et al., 1977), where the quadrupole effects are dominated by σ-bonding interactions. The second model considered the principal axis of the two tensors to be 90° apart, with the hyperfine tensor oriented in the same manner as mentioned above but with the nqi principle axis directed along the pyridine nitrogen $2p_z$ orbital. In this model, electron donation from pyridine to Co(II) would be greater than that found for the Zn complexes, and the electric field gradient at the nitrogen nucleus would be determined by the population of the p_z orbital. This second model was discounted on the basis of our ESEEM results for O_2–Co^{II}(TPP)(4-cyanopyridine) and O_2–Co^{II}(TPP)(4-carboxypyridine) which showed that the complexes containing a strong electron-withdrawing group at the para position of the pyridine ring exhibited an increased e^2qQ (see below). If the principal axis of the nqi tensor were aligned with the nitrogen $2p_z$ orbital, a decrease in e^2qQ would be expected when electron withdrawal in the π system of the pyridine is effective.

A simulation of the axial ^{14}N contribution to the O_2–Co^{II}[[^{15}N](TPP)](pyridine) ESEEM is shown in Figure 5 (dashed line) along with the data obtained for this complex (solid line). The differences between the simulation and the data are mainly due to the absence of the 0.7-MHz component, assigned to pyrrole ^{15}N coupling. The modulation depths, frequencies, and damping factors for the two higher frequency components (at 2.8 and 6.2 MHz, H = 3750 G) are correctly predicted. The nqi parameters that give a good simulation of data (e^2qQ, 2.85, and η, 0.2) are in good agreement with those found in NQR studies (Hsieh et al., 1977). The computed Fermi contact interaction is 3.5 MHz. The [^{15}N]pyrrole nitrogens are expected to yield a pair of components at 0.7 and 2.6 MHz under the experimental conditions used here, consistent with a contact coupling of 1.8 MHz.

The value of 3.5 MHz for the contact interaction of axially coordinated ^{14}N in O_2–Co^{II}[[^{15}N](TPP)](pyr) predicts that a 4.9-MHz contact should be found for the [^{15}N]pyridine case.

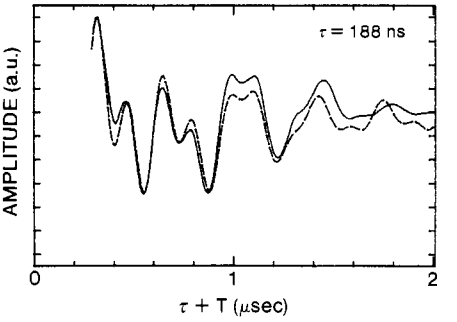

FIGURE 5: Comparison of three-pulse ESEEM data for O_2–Co^{II}-[[^{15}N](TPP)](pyridine) (solid line) with computer simulation of the pyridine ^{14}N contribution (dashed line). The data were collected under the following conditions: frequency, 10.5 GHz; magnetic field, 3750 G; pulse power, 25 W (20 ns full width at half-maximum); τ, 188 ns; temperature, 4.2 K. The Hamiltonian parameters used for the simulations were A_{xx} 2.9 MHz, A_{yy} 3.4 MHz, A_{zz} 3.9 MHz, e^2qQ 2.9 MHz, η 0.2, α 60°, β 0°, γ 0°.

Simulations of ESEEM patterns for the coordinated [^{15}N]-pyridine predict that the modulation depths would be less than 2% of the spin echo amplitude. Therefore, ESEEM due to axially bound [^{15}N]pyridine would not be seen given the signal to noise ratio of the measurement and the presence of components arising from other contributing nuclei. In fact, the ESEEM spectrum for O_2–Co^{II}[[^{15}N](TPP)][[^{15}N](pyr)] indicates that [^{15}N]pyridine gives rise to only a single component at 1.3 MHz, which is the ^{15}N Larmor frequency (Figure 4D). This component is assigned to the excess free pyridine that is "dipolar coupled" to spin.

Lower frequency components for pyrrole nitrogen in the 6-coordinate O_2–Co^{II}[[^{14}N](TPP)](L) complexes were found at 0.4, 1.26, 1.7, and 3.5 MHz.[4] Simulations of waveforms for these ESEEM data show that the modulation frequencies and their corresponding modulation depths can be predicted by using e^2qQ = 1.8 MHz, η = 0.55 (assuming nqi and hyperfine tensor alignment), and a contact interaction of 1.3

[4] The higher frequency components assigned to pyrrole nitrogen transition energies in NO–Fe^{II}(TPP)(L) data (at 3.2 and 5.5 MHz), expected to be present in the ESEEM or 6-coordinate O_2–Co^{II}(TPP)(L), are not observed because axial nitrogen coupling frequencies dominate the data in that range. A 3.5-MHz component was seen in Fourier transforms of data for O_2–Co^{II}(TPP)([^{15}N]pyr) recorded at τ = 220 ns and was also found in ESEEM spectra for O_2–Co^{II}(TPP)(methanol) in toluene (not shown). A frequency component near 5–6 MHz seen in data for NO–Fe^{II}(TPP)(L) could not be found in ESEEM of O_2–Co^{II}-(TPP)(pyr).

Table I: ESEEM Frequency Components and Calculated Magnetic Coupling Parameters for Substituted Pyridine and Imidazole Bases Axially Bound to O_2–Co^{II}(TPP)

ligand	ESEEM frequency components (MHz)	magnetic field strength (G)	calcd coupling parameters		
			a	e^2qQ	η
pyridine	1.9, 2.8, 6.2	3750	3.56 (±0.2)	2.9 (±0.2)	0.2 (±0.1)
4-methylpyridine	1.9, 2.7, 6.3	3850	3.6	2.7	0.2
4-cyanopyridine	3.3, 6.9	3900	3.9	3.4	*a*
4-carboxypyridine	2.1, 3.4, 7.2	4070	4.1	3.4	*a*
1-methylimidazole[b]	2.35, 5.6	3190	3.45	1.8	0.75
2-methylimidazole	0.8, 1.0, 1.84, 4.9	3320	2.65	1.83	0.75
4-methylimidazole[b]	1.88, 4.9	3080	2.7	1.8	0.75

[a] Only two major frequency components were resolved, precluding determination of an asymmetry parameter, which was assumed to be 0.2 for these calculations. [b] The low-frequency components, necessary to determine η, were masked for these samples because of ESEEM due to [^{14}N]TPP. The calculations assumed that an asymmetry parameter value of 0.75, determined for 2-methylimidazole, was correct for these complexes as well.

MHz. (Simulated waveforms are not shown.) The nqi parameters are in good agreement with those reported for Ag(TPP) by Brown and Hoffman (1980), and the magnitude of the contact interaction is consistent with that predicted from components seen in ESEEM spectra of the O_2–Co^{II}[[^{15}N](TPP)] complex. The wide line width of the 3.5-MHz component requires that the anisotropy in the hyperfine tensor be large. If the tensor is taken to be axial with A_{xx}, $A_{yy} = a - F$, and $A_{zz} = a + 2F$, F must be at least 0.3 MHz.

An extended series of 6-coordinate O_2–Co^{II}(TPP)(L) complexes was also investigated, with L = 4-cyanopyridine, 4-carboxypyridine, 4-picoline, and 1-, 2-, and 4-methylimidazole. The ESEEM data obtained at 11 GHz for the complexes prepared with Co^{II}[[^{15}N](TPP)] and the calculated contact couplings and e^2qQ values for axial nitrogen are summarized in Table I. The lower e^2qQ values found for the stronger bases are in agreement with the model put forth by Hsieh et al. (1977): The stronger bases donate more lone pair electron density through a σ bond to the cobalt, which lowers the e^2qQ value from that of noncoordinated base by a larger amount compared to that for the weaker bases. The trend also indicates stronger contact coupling for the axially bound nitrogen of the weaker base ligands. Similar trends in contact couplings and quadrupole parameters are seen for the imidazole complexes. It was possible to simulate the ESEEM data for all three imidazole ligands with the same set of nqi parameters (e^2qQ 1.83 MHz, η 0.75), where the principal axis of both hyperfine and nqi tensors were taken to be aligned. These values are in excellent agreement with the predictions based on NQR studies of Zn(II)–imidazole complexes (Ashby et al., 1978). (The small e^2qQ and larger η values for the imidazoles reflects the greater π electron density in the five-membered heterocycle ring compared to that in pyridine.) The magnitude of the contact interaction for the 2-methyl- and 4-methylimidazole cases was found to be much less than that calculated for the 1-methylimidazole case. This trend is again consistent with the greater basicity of 2- and 4-methylimidazole compared to that of 1-methylimidazole. Steric effects that might be introduced by the methyl group at the 2-position are probably not important since no difference was found between the ^{14}N couplings in 2- and 4-picoline complexes or the 2- and 4-methylimidazole complexes of O_2–CO^{II}(TPP)(L). (Data for 2-picoline are not shown.)

The oxy cobaltous porphyrins are low-spin d^7 complexes whose EPR properties have been discussed in earlier literature (Walker, 1970; Hoffman, 1970; Wayland et al., 1974; Tovrog et al., 1976). The lack of nitrogen hyperfine information from continuous wave EPR experiments for 6-coordinate oxygenated complexes makes complete description of the magnetic properties difficult, though stronger bases give slightly smaller ^{59}Co couplings (Walker, 1970). The smaller cobalt hyperfine coupling is consistent with less spin density in cobalt orbitals when the axial ligand is a strong base. In a model for these complexes that considers "oxygenation" to be equivalent to "oxidation" (Hoffman et al., 1970; Burness et al., 1975), electron transfer from Co(II) to O_2 occurs, and hyperfine interactions arise from transfer of unpaired spin from the bound superoxide back into cobalt and the axial nitrogen. The magnitude of the interactions would then be predicted to diminish in complexes in which electron pair donation from axial nitrogen was effective (i.e., for strong bases) since electron transfer is facilitated.

A more comprehensive treatment of the origin of hyperfine interactions using a molecular orbital treatment of bonding in oxy cobaltous complexes suggests that upon oxygenation spin pairing occurs between the single electron in the cobalt d_{z^2} orbital and a π^* electron from oxygen (Tovrog et al., 1976). A σ-bonding molecular orbital is formed by combination of d_{z^2} with an oxygen π^* orbital and a small contribution from cobalt 4s. Hyperfine interactions then arise from polarization of this filled bonding orbital by the unpaired spin remaining on oxygen. In this scheme, lone pair donation from axial bases would tend to destabilize d_{z^2}, giving the σ-bonding orbital more O_2 character and resulting in smaller hyperfine interactions in the cobalt and thereby in the axial nitrogen. The hyperfine interaction would then improve for the poorer donors, which is reflected by the increasing contact interaction shown in the data summarized in Table I.

The improved contact coupling in the pyridines having strongly electronegative para substituents may also reflect the better π-acceptor nature of the weaker base ligands. The induction of π density from the ring could improve the metal to ligand ($d\pi$–$p\pi$) donation and thereby increase the unpaired spin density in the coordinating nitrogen. This effect, however, competes with an expected decreased hyperfine interaction when $d\pi$–$p\pi$ overlap is improved since the separation between d_{xz} and d_{yz} orbitals and the π^* orbital containing the unpaired electron should increase when the $d\pi$ orbitals are lowered in energy. The data may be taken to suggest that the lowering of $d\pi$ orbital energies does not dominate the increased hyperfine interactions due to increased unpaired spin density in the axial nitrogen with improved overlap. The models described are comprehensive enough to explain the trends in the ESEEM data without consideration of changes in oxygen binding energies, which would also influence the transfer of unpaired spin through cobalt to axial nitrogen. The trends in oxygen binding energy in the series of complexes is expected to parallel base strength and, therefore, strong bases would still be predicted to give weaker hyperfine interactions and good oxygen bond strength.

Conclusions. In summary, we have shown that ESEEM spectroscopy can be used to examine electron–nuclear coupling

in NO-Fe^{II}(TPP)(L) complexes, in nitrosyl heme proteins, and in the isoelectronic O_2-Co^{II}(TPP)(L) complexes. Magnetic coupling to pyrrole nitrogen in all cases is nearly the same. The coupling to axial nitrogen in the oxygenated cobalt complexes reveals a trend toward stronger hypefine interaction with weaker base ligands.

Registry No. Nitrosyl-HbA, 52228-24-7; NO-Fe^{II}(TPP), 52674-29-0; NO-Fe^{II}(TPP)(pyridine), 53637-83-5; NO-Fe^{II}(TPP)(imidazole), 110970-92-8; O_2-Co^{II}(TPP), 37249-49-3; O_2-Co^{II}(TPP)(pyridine), 60470-41-9; O_2-Co^{II}(TPP)(4-methylpyridine), 80976-85-8; O_2-Co^{II}(TPP)(4-cyanopyridine), 110970-93-9; O_2-Co^{II}(TPP)(4-carboxypyridine), 110934-25-3; O_2-Co^{II}(TPP)(1-methylimidazole), 93222-64-1; O_2-Co^{II}(TPP)(2-methylimidazole), 110970-94-0; O_2-Co^{II}(TPP)(4-methylimidazole), 110934-26-4; heme, 14875-96-8.

References

Ascenzi, P., Giacometti, G. M., Antonini, E., Rotilio, G., & Brunori, M. (1981) *J. Biol. Chem. 256*, 5383–5386.

Ashby, C. I. H., Cheng, C. P., & Brown, T. L. (1978) *J. Am. Chem. Soc. 100*, 6057–6067.

Bayston, J. H., King, N. K., Looney, F. D., & Winfield, M. E. (1969) *J. Am. Chem. Soc. 91*, 2775–2779.

Blumberg, W. E., Peisach, J., Wittenberg, B. A., & Wittenberg, J. (1968) *J. Biol. Chem. 243*, 1854–1862.

Bonaventura, J., & Bonaventura, C. (1981) *Methods Enzymol. 76*, 5–29.

Boyer, P. D. (1954) *J. Am. Chem. Soc. 76*, 4331–4337.

Britt, R. D., & Klein, M. P. (1987) *J. Magn. Reson.* (in press).

Brown, T. G., & Hoffman, B. M. (1980) *J. Mol. Phys. 39*, 1073–1109.

Bucci, E. (1981) *Methods Enzymol. 76*, 97–106.

Burness, J. H., Dillard, J. G., & Taylor, L. T. (1975) *J. Am. Chem. Soc. 97*, 6080–6088.

Carrico, R. J., Peisach, J., Alben, J. O. (1978) *J. Biol. Chem. 253*, 2386–2391.

Chevion, M., Peisach, J., & Blumberg, W. E. (1977) *J. Biol. Chem. 252*, 3637–3645.

Drago, R. S., Beugelsdijk, T., Breese, J. A., Cannady, J. P. (1978) *J. Am. Chem. Soc. 100*, 5374–5382.

Geraci, G., Parkhurst, L. J., & Gibson, Q. H. (1969) *J. Biol. Chem. 244*, 4664–4667.

Getz, D., Malamud, E., Silver, B. L., & Dori, Z. (1975) *J. Am. Chem. Soc. 97*, 3846–3847.

Guibé, L. (1962) *Ann. Phys. (Paris) 7*, 177.

Hille, R., Olson, J. S., & Palmer, G. (1979) *J. Biol. Chem. 254*, 12110–12120.

Hoffman, B. M., Diemente, D. L., & Basolo, F. (1970) *J. Am. Chem. Soc. 92*, 61–65.

Höhn, M., Hütterman, J., Chien, J. C. W., & Dickinson, L. C. (1983) *J. Am. Chem. Soc. 105*, 109–115.

Hollenberg, P. F., Hager, L. P., Blumberg, W. E., & Peisach, J. (1980) *J. Biol. Chem. 255*, 4801–4807.

Hori, H., Ikeda-Saito, M., & Yonetani, T. (1981) *J. Biol. Chem. 256*, 7849–7855.

Hsieh, Y.-N., Rubenacker, G. V., Cheng, C. P., & Brown, T. L. (1977) *J. Am. Chem. Soc. 99*, 1384–1389.

Ikeda-Saito, M., Inubushi, T., & Yonetani, T. (1981) *Methods Enzymol. 76*, 113–121.

Kevan, L. (1979) in *Time Domain Electron Spin Resonance* (Kevan, L., & Schwartz, R. N., Eds.) pp 279–342, Wiley-Interscience, New York.

Kon, H. (1968) *J. Biol. Chem. 243*, 4350–4357.

Kon, H. (1975) *Biochim. Biophys. Acta 379*, 103–113.

Kon, H., & Kataoka, N. (1969) *Biochemistry 8*, 4757–4762.

Kosman, D. J., Peisach, J., & Mims, W. B. (1980) *Biochemistry 19*, 1304–1308.

Lin, C. P., Bowman, M. K., & Norris, J. R. (1985) *J. Magn. Reson. 65*, 369–374.

LoBrutto, R., Wei, Y.-H., Mascarenhas, R., Scholes, C. P., & King, T. E. (1983) *J. Biol. Chem. 258*, 7437–7448.

McCracken, J., Dooley, D. M., & Peisach, J. (1987a) *J. Am. Chem. Soc. 109*, 4064–4072.

McCracken, J., Pember, S. O., Benkovic, S. J., Villafranca, J. J., Miller, R. J., & Peisach, J. (1987b) *Biochemistry* (in press).

Mims, W. B. (1972) *Phys. Rev. B: Solid State B5*, 2409–2419.

Mims, W. B. (1974) *Rev. Sci. Instrum. 45*, 1583–1591.

Mims, W. B. (1984) *J. Magn. Reson. 59*, 291–306.

Mims, W. B., & Peisach, J. (1976) *Biochemistry 15*, 3863–3869.

Mims, W. B., & Peisach, J. (1978) *J. Chem. Phys. 69*, 4921–4930.

Mims, W. B., & Peisach, J. (1979) in *Biological Applications of Magnetic Resonance* (Shulman, R. G., Ed.) pp 221–269, Academic, New York.

Morse, R. H., & Chan, S. I. (1980) *J. Biol. Chem. 255*, 7876–7882.

Mun, S. K., Chang, J. C., & Das, T. P. (1979) *Proc. Natl. Acad. Sci. U.S.A. 76*, 4842–4846.

Nagai, K., Welborn, C., Dolphin, D., & Kitagawa, T. (1980) *Biochemistry 19*, 4755–4761.

Palmer, G. (1985) *Biochem. Soc. Trans. 13*, 548–560.

Peisach, J. (1982) in *Oxidases and Related Redox Systems* (King, T. E., Mason, H. S., & Morrison, M., Eds.) pp 575–596, Pergamon, New York.

Peisach, J., Blumberg, W. E., Ogawa, S., Rachmilewitz, E. A., & Oltzick, R. (1971) *J. Biol. Chem. 246*, 3342–3355.

Peisach, J., Mims, W. B., & Davis, J. (1979) *J. Biol. Chem. 254*, 12379–12389.

Peisach, J., Mims, W. B., & Davis, J. (1984) *J. Biol. Chem. 259*, 2704–2706.

Reijerse, E. J., & Keijzers, C. P. (1987) *J. Magn. Reson. 71*, 83–96.

Rillema, D. P., Wicker, C. M., Jr., Morgan, R. D., Barringer, L. F., & Scism, L. A. (1982) *J. Am. Chem. Soc. 104*, 1276–1281.

Scheidt, W. R., & Frisse, M. E. (1975) *J. Am. Chem. Soc. 97*, 17–21.

Stynes, D. V., Stynes, H. C., James, B. R., & Ibers, J. A. (1973) *J. Am. Chem. Soc. 95*, 1796–1801.

Szabo, A., & Perutz, M. (1976) *Biochemistry 15*, 4427–4428.

Tovrog, B. S., Kitko, D. J., & Drago, R. S. (1976) *J. Am. Chem. Soc. 98*, 5144–5153.

Townes, C. H., & Dailey, B. P. (1949) *J. Chem. Phys. 17*, 782–796.

Van Camp, H. L., Sands, R. H., & Fee, J. A. (1981) *J. Chem. Phys. 75*, 2098–2107.

Walker, F. A. (1970) *J. Am. Chem. Soc. 92*, 4235–4244.

Wayland, B. B., Minkiewicz, J. V., & Abd-Elmageed, M. E. (1974) *J. Am. Chem. Soc. 96*, 2795–2801.

Yonetani, T., Yamamoto, H., Herman, J. E., Leigh, J. S., Jr., & Reed, G. H. (1972) *J. Biol. Chem. 247*, 2447–2455.